

# Spectral Methods in General Relativity and Large Randall-Sundrum II Black Holes

Shohreh Abdolrahimi,<sup>a,b</sup> Céline Cattoën,<sup>a,c</sup> Don N. Page,<sup>a</sup>  
Shima Yaghoobpour-Tari<sup>a</sup>

<sup>a</sup>Department of Physics, 4-181 CCIS, University of Alberta, Edmonton, Alberta T6G 2E1, Canada

<sup>b</sup>Institut für Physik, Universität Oldenburg, Postfach 2503 D-26111 Oldenburg, Germany

<sup>c</sup>BlueFern Supercomputing Unit, University of Canterbury, Christchurch 8140, New Zealand

E-mail: [abdolah@ualberta.ca](mailto:abdolah@ualberta.ca), [celine.cattoen-gilbert@canterbury.ac.nz](mailto:celine.cattoen-gilbert@canterbury.ac.nz),  
[dpage@ualberta.ca](mailto:dpage@ualberta.ca), [yaghoobp@ualberta.ca](mailto:yaghoobp@ualberta.ca),

[Alberta Thy 14-12](#)

**Abstract.** Using a novel numerical spectral method, we have found solutions for large static Randall-Sundrum II (RSII) black holes by perturbing a numerical AdS<sub>5</sub>-CFT<sub>4</sub> solution to the Einstein equation with a negative cosmological constant  $\Lambda$  that is asymptotically conformal to the Schwarzschild metric. We used a numerical spectral method independent of the Ricci-DeTurck-flow method used by Figueras, Lucietti, and Wiseman for a similar numerical solution. We have compared our black-hole solution to the one Figueras and Wiseman have derived by perturbing their numerical AdS<sub>5</sub>-CFT<sub>4</sub> solution, showing that our solution agrees closely with theirs. We have also deduced the new results that to first order in  $1/(-\Lambda M^2)$ , the Hawking temperature and entropy of an RSII static black hole have the same values as the Schwarzschild metric with the same mass, but the horizon area is increased by about  $4.7/(-\Lambda)$ .

**Keywords:** gravity, modified gravity, and astrophysical black holes

**Date:** Mayan Long Count Calendar 13.0.0.0.0, or day 1,872,000, end of the 13th b'ak'tun (2012 Dec. 21 in the Gregorian Calendar)

---

## Contents

<b>1</b>	<b>Introduction</b>	<b>1</b>
<b>2</b>	<b>Infinite Black Hole Metric</b>	<b>3</b>
<b>3</b>	<b>Finite Black Hole Metrics</b>	<b>9</b>
<b>4</b>	<b>RSII black hole metric on the brane</b>	<b>12</b>
<b>5</b>	<b>Conclusion</b>	<b>19</b>
<b>A</b>	<b>Explicit Form of Functions</b>	<b>20</b>

---

## 1 Introduction

In this paper we consider the Randall-Sundrum II (RSII) [1] model, which is a five-dimensional gravitational model. The idea of extra dimensions goes back to 1914, when Nordström made an unsuccessful attempt to describe gravity and electromagnetism simultaneously by introducing one extra spatial dimension [2]. His theory did not turn out to be correct and was replaced by Einstein's theory. Later, Kaluza's work gave birth to the modern Kaluza-Klein (KK) theories [3, 4]. Kaluza considered a five-dimensional spacetime with one additional spatial dimension to unify the fundamental forces of gravity and electromagnetism. Initially these theories were rather a mathematical exercise. The formulation of string theory and M-theory in a space-time with a number of dimensions greater than four has provided more support for the idea of higher dimensions. At first, the size of these extra dimensions was naturally considered to be of the order of Planck length,  $l_{pl} \sim 10^{-33}$  cm. This is because in KK theories, using extra compact dimensions, a tower of four-dimensional particles with masses proportional to the inverse size of the compact dimension  $L^{-1}$  are produced. However, the standard model has been successfully tested up to  $\sim 100$  GeV. In 1983 Rubakov and Shaposhnikov [5] proposed a novel model in which fermions and bosons are confined to a four-dimensional subspace of a higher dimensional space-time. Following a similar direction, D-branes have been introduced in string theory [6], where fermions, bosons and gauge fields associated with open strings are confined to propagate only along the brane, while gravity, associated with closed strings, can propagate in the bulk. This gave rise to the so-called braneworld models. In simple words a braneworld is a slice through spacetime on which we live and where our standard model physics is confined. Braneworld scenarios also provide a geometrical interpretation of the hierarchy problem, where the electroweak scale  $m_{EW} \sim 1$  TeV is much smaller than the Planck scale  $M_{Pl} = G^{-1/2} = 1.2 \times 10^{16}$  TeV. Two of the most popular braneworld models are those of Randall and Sundrum [1, 7].

In the Randall-Sundrum (RS) models our world is considered as a brane or a domain wall embedded in a five-dimensional spacetime with a negative cosmological constant. The Randall-Sundrum model II (RSII) [1] has one domain wall, situated in a five-dimensional bulk asymptotically anti-de Sitter (AdS) space-time. The ground state bulk metric is precisely AdS on each side of the brane at  $w = 0$ ,

$$ds^2 = \frac{l^2}{(l + |w|)^2} [dw^2 - dt^2 + dx_1^2 + dx_2^2 + dx_3^2], \quad (1.1)$$

where  $l$  is the curvature length scale of the negatively curved five-dimensional AdS space-time, related to the bulk cosmological constant by  $l^2 = -6/\Lambda$ . This bulk metric satisfies the five-dimensional Einstein equations with a cosmological constant

$$G_{\mu\nu} = -\Lambda g_{\mu\nu}, \quad \text{or} \quad R_{\mu\nu} = \frac{2}{3}\Lambda g_{\mu\nu}. \quad (1.2)$$

Each slice of  $w = \text{const.}$  represents a flat four-dimensional space-time. The conformal factor, which depends on  $w$  alone in this case, is known as the warp factor. At  $w = 0$  we have the flat Minkowski metric of a domain wall, or brane. This brane is an infinitely thin brane, which satisfies the Israel junction condition

$$[K_{\mu\nu}] = -\frac{2}{l}\gamma_{\mu\nu}, \quad (1.3)$$

where  $[K_{\mu\nu}]$  is the difference of the extrinsic curvature of the brane on the two sides ( $w < 0$  and  $w > 0$ ) and  $\gamma_{\mu\nu}$  is the induced metric on the brane at  $w = 0$ . The brane tension is  $\sigma = 3/(4\pi l G_5)$ , where  $G_5$  is the five-dimensional Newton's constant. The bulk Einstein equation plus the Israel junction condition for a brane with the RSII value of the tension and without matter imply that the Ricci scalar of the brane metric is zero for a general asymmetric static metric. Applying linear perturbation theory for the metric (1.1) shows that a Newtonian potential can be reproduced, so four-dimensional gravity is recovered for this theory.

One important question is whether the RSII model can describe our universe. For the RSII model to be a candidate for describing our universe, it must admit black hole solutions. There has been much debate, and various conjectures and claims in the last few years, about the existence of a static black hole solution within the RSII model. An exact black hole solution was found for the dimension  $d = 4$  of the bulk spacetime, where the static black hole is localized on a 2-brane [8], using the so-called C metric [9]. In [10, 11] it was conjectured that based on the AdS/CFT correspondence large static five-dimensional black hole cannot exist. According to [10], such bulk black holes would necessarily be time dependent, since their duals would describe quantum corrected black holes in a  $d - 1$  dimensional braneworld. However, counterarguments were given in [12]. In [13, 14] nontrivial localized black hole solutions have been found numerically, whose horizon radii were small compared to the bulk curvature scale. In their formulation, the problem was reduced to elliptic equations for metric functions with appropriate boundary conditions. They solved this problem by a relaxation method. Although their method has worked well for the small localized black holes, they could not succeed in finding black hole solutions with large horizon radius. In fact as the mass of the black hole became large, the convergence became worse and the error grew. One can consider the results [13, 14] as evidence for the existence of solutions of a black hole on a brane with a small mass. However, the other interpretation suggested in [15] was that maybe that the growth of the error can be regarded as evidence for the nonexistence of such solutions. Therefore [15] took the task of re-examining of the result of [13, 14], numerically developing a code having an almost 4th-order accuracy. According to the author, this code derived a highly accurate result for the case where the brane tension was zero, i.e., the spherically symmetric case. However, a nonsystematic error was detected in the cases where the brane tension was nonzero. This error was irremovable by any systematic methods such as increasing the resolution, setting the outer boundary at more distant location, or improving the convergence of the numerical relaxation. Thus, it was suggested in [15] that a solution sequence of a static

black hole on an asymptotically flat brane that is reduced to the Schwarzschild black hole in the zero tension limit is unlikely to exist. In [16] the result of [13, 14, 15] was re-examined again employing a different numerical methods, and the result of [15] was confirmed. For other discussions see [17, 18, 19, 20, 21, 22].

Despite all these claims, Figueras and Wiseman [23] (henceforth FW) recently found such solutions by perturbing an AdS<sub>5</sub>-CFT<sub>4</sub> solution that Figueras, Lucietti, and Wiseman [24] (henceforth FLW) had found earlier by Ricci-DeTurck flow. This AdS<sub>5</sub>-CFT<sub>4</sub> metric is a solution to the Einstein equations with a negative cosmological constant  $\Lambda$  that is asymptotically conformal to the Schwarzschild metric. Because the Schwarzschild metric appears at an AdS<sub>5</sub> boundary with an infinite scale factor, it may be viewed as a black hole of infinite mass.

We had independently searched for and found the infinite-mass black hole solution by a different numerical method and were preparing to perturb it to get large-mass RSII black hole solutions when the Figueras et al. papers appeared. Here expanding upon [25], we report that our numerical solution agrees well with that of Figueras et al. and thus helps to support the existence of large RSII black holes, despite the doubts expressed by previous work. We point out here that the previous results of [13, 14, 15, 16] have been concentrated on the small black hole regime.

We used a spectral method, expressing the components of the 5-dimensional metric in terms of Legendre polynomials in the two nontrivial coordinates, with the appropriate boundary conditions imposed. We chose the 210 coefficients of the polynomials to minimize the integrated square of the error of the Einstein equation. We have reduced the integrated square of the error of the Einstein equation by eight orders of magnitude from the case with no free parameters (constant polynomials). This strongly suggests that we are numerically near an exact solution, though of course our limited computational resources meant that we could not use an infinite number of parameters to reduce the numerical error all the way to zero. The integrated square error is based on the Gauss-Legendre quadrature numerical method, and the minimization procedure uses the simplex search method for multivariable functions. This approach to solving the Einstein equations is novel, and the good agreement of our results with the Figueras et al. results illustrates the success of the method, especially in comparison with the failure of various previous numerical attempts.

We present an explicit approximate metric for the black hole on the brane. Using this approximate metric we demonstrate that the area of an RSII black hole on the brane is slightly greater than a black hole in pure four-dimensional general relativity, and to leading order, the relations between the mass, Hawking temperature, and Bekenstein-Hawking entropy are precisely the same as in four-dimensional general relativity.

## 2 Infinite Black Hole Metric

The first attempt for finding a black hole solution in the RS model was that of Chamblin, Hawking and Reall [26]. They have replaced the Minkowski metric in (1.1) with the Schwarzschild metric; one can in fact replace it with any 4-dimensional Ricci-flat metric. The result is

$$ds^2 = \frac{l^2}{w^2} [dw^2 - U(r)dt^2 + U(r)^{-1}dr^2 + r^2d\Omega^2], \quad (2.1)$$

where  $U(r) = 1 - 2M/r$  and where  $d\Omega^2 = d\theta^2 + \sin^2\theta d\phi^2$  is the unit two-sphere metric. Letting  $r = 2M/y$  and  $w = 2M/v$  and setting  $l = 1$  gives

$$ds^2 = \frac{dv^2}{v^2} + \frac{v^2 dy^2}{y^4(1-y)} - 4v^2(1-y)dt^2 + \frac{v^2}{y^2}d\Omega^2. \quad (2.2)$$

The hypersurfaces of constant  $v$  are Schwarzschild metrics of mass  $m(v) = v/2$ . The curvature at  $y > 0$  diverges at  $v = 0$ , so this black string metric is singular. We modify the metric by adding some  $y^2$  terms to remove this singularity, and we also introduce four metric functions to give

$$ds^2 = A \frac{dv^2}{v^2 + y^2} + B \frac{(v^2 + y^2)dy^2}{y^4(1-y)} - 4C(v^2 + y^2)(1-y)dt^2 + D \frac{v^2}{y^2}d\Omega^2. \quad (2.3)$$

We then replace  $v$ , which ranges from 0 to  $\infty$ , by  $x = y^2/(y^2 + v^2)$ , so that the metric becomes

$$ds^2 = A(1-x) \left[ \frac{dx}{2x(1-x)} - \frac{dy}{y} \right]^2 + B \frac{dy^2}{xy^2(1-y)} - 4C \frac{y^2(1-y)}{x} dt^2 + D \frac{1-x}{x} d\Omega^2, \quad (2.4)$$

where  $0 \leq x \leq 1$ ,  $0 \leq y \leq 1$  and  $A(x, y)$ ,  $B(x, y)$ ,  $C(x, y)$  and  $D(x, y)$  are smooth functions of  $x$  and  $y$ . The coordinate boundaries are these:  $x = 0$  is the infinite AdS boundary that is conformal to the Schwarzschild metric when we impose  $A = B = C = D = 1$  there,  $y = 0$  is the extremal Poincare horizon,  $x = 1$  is the axis of symmetry where the two-sphere shrinks to zero size and where we impose  $A = D$  for regularity, and  $y = 1$  is the black hole horizon where we impose the regularity requirement  $B = C$ .

In the rest of this paper we choose units in which  $l = 1$ , or  $\Lambda = -6$ . We impose these regularity conditions and also solve the Einstein equations to lowest order in  $x$  by writing  $A$ ,  $B$ ,  $C$ , and  $D$  in terms of polynomial functions of  $x$  and/or  $y$ ,  $f(y)$ ,  $g(y)$ ,  $\tilde{A}(x, y)$ ,  $\tilde{B}(x, y)$ ,  $\tilde{C}(x, y)$ , and  $\tilde{D}(x, y)$  with the following forms:

$$\begin{aligned} A &= 1 - x(1-x)(1+2f) + x^2g + x^2(1-x)\tilde{A}, \\ B &= 1 + xf + x^2\tilde{B}, \\ C &= 1 + xf + x^2\tilde{B} + x^2(1-y)\tilde{C}, \\ D &= 1 + x(1-x)(1+f) + x^2g + x^2(1-x)\tilde{D}. \end{aligned} \quad (2.5)$$

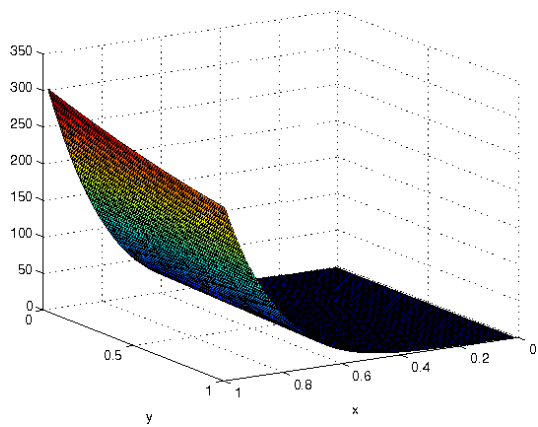
Our goal is to find the six functions  $f$ ,  $g$ ,  $\tilde{A}$ ,  $\tilde{B}$ ,  $\tilde{C}$ , and  $\tilde{D}$  such that (2.4) solves the Einstein equation (1.2). To achieve this numerically, we use an optimization method. We first define

$$E_{\mu\nu} = R_{\mu\nu} + 4g_{\mu\nu}, \quad (2.6)$$

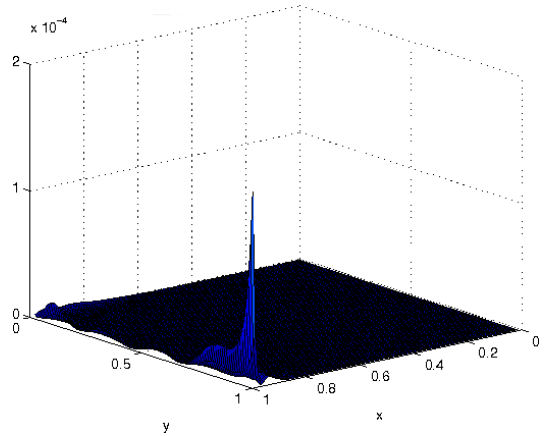
which should be zero for a solution to the Einstein equation. Then we define the integrated square error as

$$I = \int \sqrt{-{}^{(5)}g} E_{\mu\nu} E^{\mu\nu} d^5x, \quad (2.7)$$

where this integral is taken over  $0 \leq x \leq 1$ ,  $0 \leq y \leq 1$ ,  $0 \leq \theta \leq \pi$ ,  $0 \leq \phi \leq 2\pi$ , and where we choose  $\Delta t = 2\pi$ , i.e. the period of an imaginary time coordinate  $\tau = it$  avoiding a conical singularity at the horizon location  $y = 1$ . Assuming that  $E_{\alpha\beta} E^{\alpha\beta}$  falls off fast enough toward the infinite AdS boundary at  $x = 0$ , where the metric determinant  ${}^{(5)}g \propto 1/x^6$  diverges, the integral converges. Note that for a static metric, the integrand of (2.7) is positive semidefinite,

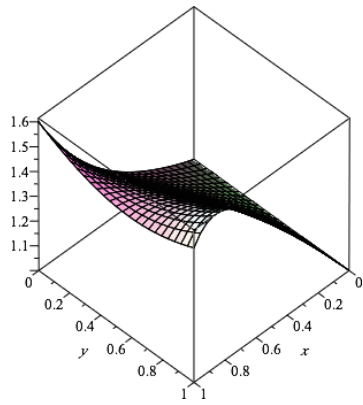


(a)  $A = B = C = D = 1$

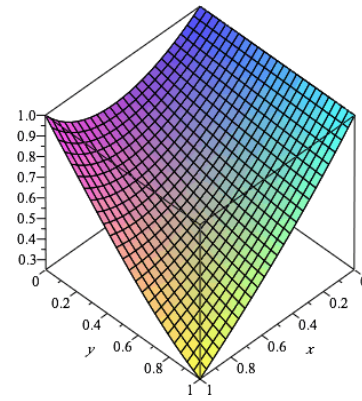


(b) 6th-order

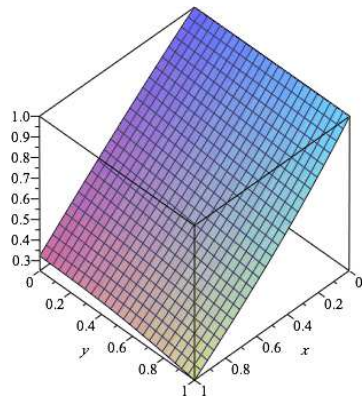
Figure 1.  $E_{\mu\nu}E^{\mu\nu}$  vs.  $x$  and  $y$



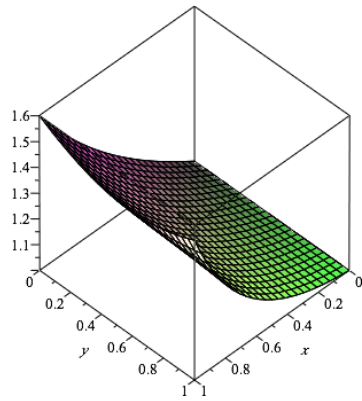
(a)  $A(x,y)$



(b)  $B(x,y)$



(c)  $C(x,y)$



(d)  $D(x,y)$

Figure 2. The functions  $A$ ,  $B$ ,  $C$ , and  $D$  vs.  $x$  and  $y$ .

	coefficients	I
$A = B = C = 1$	0	4038
0th-order	6	69.6986
1st-order	20	1.5656
2nd-order	42	$4.7786 \times 10^{-1}$
3th-order	72	$2.3903 \times 10^{-2}$
4th-order	110	$2.5352 \times 10^{-3}$
5th-order	156	$5.4220 \times 10^{-4}$
6th-order	210	$4.2385 \times 10^{-4}$

**Table 1.** The value of  $I$ , Eq. (2.7), vs. the change in the order of the polynomial expansion for the functions  $\tilde{A}$ ,  $\tilde{B}$ ,  $\tilde{C}$ ,  $f$ , and  $g$ . Changing the order of the polynomial the number of coefficients which need to be modified change according to the second column.

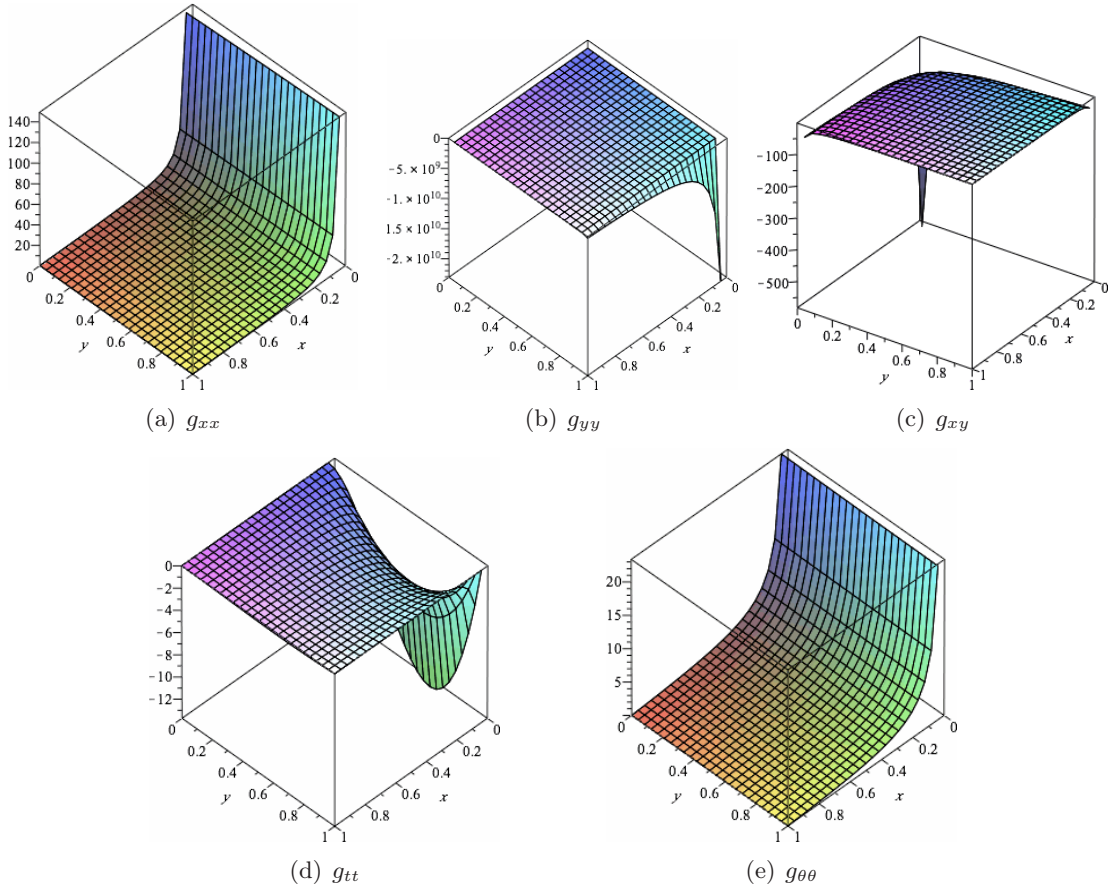


**Figure 3.** Metric functions.

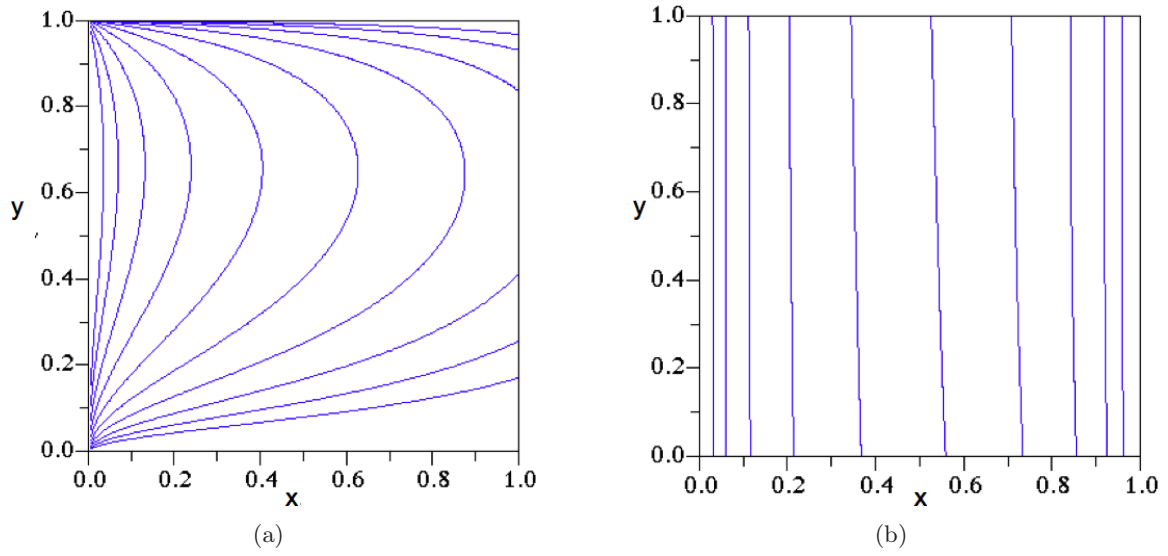


**Figure 4.** (a) Contour lines of constant  $g_{tt}$ . The curves from left to right have  $g_{tt}$  going from 16 on the left down to  $1/32$  on the right with each curve having half the value of the one to its left. (b) Contour lines of constant  $g_{\theta\theta}$ . The curves from left to right have  $g_{\theta\theta}$  going from 32 on the left down to  $1/16$  on the right with each curve having half the value of the one to its left.

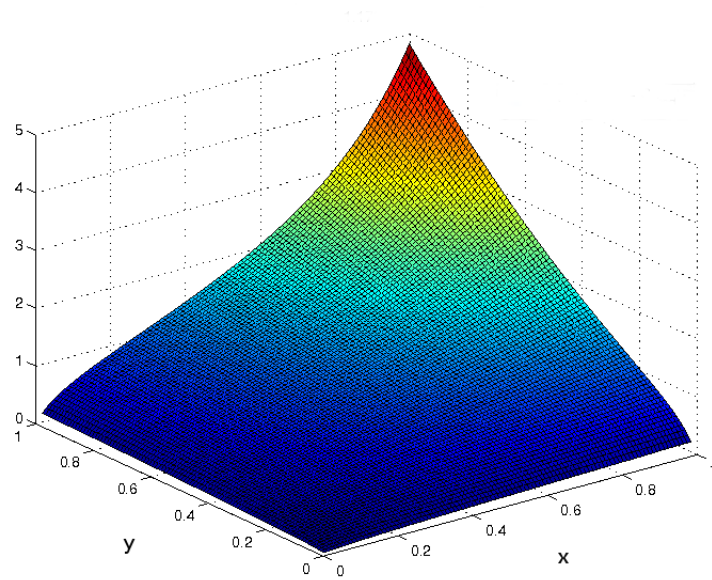


**Figure 5.** Fourth root of the trace of the square of the Weyl tensor  $\mathcal{C}^{1/4}$  as a function of  $x$  and  $y$ .



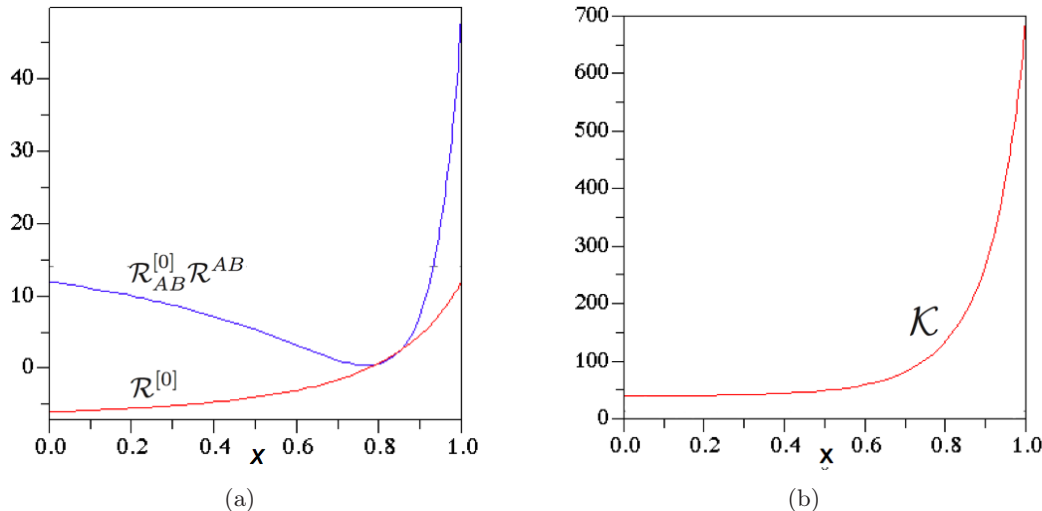


**Figure 6.** (a) Ricci scalar and the square of Ricci tensor of the horizon surface vs.  $x$ . (b) Space-time Kretschmann scalar calculated on the horizon vs.  $x$ .

so for a smooth metric, the error integral  $I$  will vanish only if one has a solution to the Einstein equation.

We assume the functions  $f$ ,  $g$ ,  $\tilde{A}$ ,  $\tilde{B}$ ,  $\tilde{C}$ , and  $\tilde{D}$  to be polynomial functions of  $x$  and  $y$ , and then try to minimize  $I$ . For the integration method, we use the Gauss-Lobatto quadrature in two dimensions, and for the optimization method we use an unconstrained nonlinear optimization. We have considered a Taylor series expansion, a shifted-Legendre expansion, and a Pade-Legendre expansion of the  $f$ ,  $g$ ,  $\tilde{A}$ ,  $\tilde{B}$ ,  $\tilde{C}$ , and  $\tilde{D}$  functions in  $x$  and  $y$ . The Taylor expansion gave a slow rate of convergence for the optimization. The shifted-Legendre and Pade-Legendre give comparable rates; however, Pade-Legendre has a more complicated form. Thus, the shifted-Legendre series expansion, which is defined on the interval  $[0, 1]$ , gives the best result among the three. This is what we chose for our computations. We start with the case where  $f = g = \tilde{A} = \tilde{B} = \tilde{C} = \tilde{D} = 0$ , in other words  $A = B = C = D = 1$ . This gives the error integral  $I \approx 4038$ . Then we increase the order of polynomial expansion gradually. The 0th-order polynomial expansion gave a minimum  $I \approx 69.6986$ . For each order, we run the optimization procedure a few times until the value of the integral  $I$  remains almost a constant. Table 1 shows the final values of  $I$  with increasing order of polynomials. Using the 6th-order polynomial expansion of  $f$ ,  $g$ ,  $\tilde{A}$ ,  $\tilde{B}$ ,  $\tilde{C}$ , and  $\tilde{D}$ , with a total of 210 coefficients, the integrated squared error was reduced to 0.0004238, nearly eight orders of magnitude smaller than when  $A = B = C = D = 1$ . Our numerical accuracy is  $10^{-10}$ . The resulting functions  $f$ ,  $g$ ,  $A$ ,  $B$ ,  $C$ , and  $D$  are given in Appendix A. The maximum value of the squared error at any point within the 5-dimensional space-time was then  $E_{\alpha\beta}E^{\alpha\beta} = 0.000154$ , as shown in Fig 1. Thus, we appear to have strong evidence that our numerical method is converging toward an exact solution of the infinite black hole metric. Due to a finite amount of resources and time, we have stopped at this order. We have calculated the fourth root of the trace of the square of the Weyl tensor,  $\mathcal{C}^{1/4} = (C_{\alpha\beta\gamma\delta}C^{\alpha\beta\gamma\delta})^{1/4}$ , for our metric (2.4). Because our metric uses different coordinates from those used by FLW, it is not easy to make many comparisons over the entire bulk five-dimensional manifold. We have found that the value for the fourth root of the square of the Weyl tensor,  $(C_{\alpha\beta\gamma\delta}C^{\alpha\beta\gamma\delta})^{1/4}$  at the corner  $x = 1$ ,  $y = 1$  (the intersection of the black hole horizon with the axis) to be 4.863 in our metric, which is reasonably

near the 5.064 that FLW privately reported to us from their metric. We shall make many more comparisons below for the four-dimensional large black hole metric.

The metric of a  $t = \text{const}$  cross section of the horizon surface at  $y = 1$  is

$$ds_3^2 = g_{AB}dx^A dx^B = \frac{A(x)}{4x^2(1-x)}dx^2 + \frac{D(x)(1-x)}{x}d\Omega^2, \quad (2.8)$$

with

$$A(x) = 1 + 0.85959x + 0.221970x^2 - 0.66519x^3 + 0.63763x^4 - 0.97718x^5 \\ + 1.53365x^6 - 0.96168x^7 - 0.29554x^8 + 0.18927x^9, \quad (2.9)$$

$$D(x) = 1 + 0.07021x + 0.14336x^2 + 0.22442x^3 - 0.15951x^4 + 0.54809x^5 \\ - 0.71742x^6 + 0.60302x^7 - 0.19459x^8 + 0.02494x^9. \quad (2.10)$$

We have calculated the Ricci scalar  $\mathcal{R}$  and the trace of the square of the Ricci tensor,  $\mathcal{R}_{AB}\mathcal{R}^{AB}$ , of the horizon surface in Fig 6(a). The Ricci scalar at  $x = 0$  is  $-6$  and is equal to 12.17095 at  $x = 1$ . The square of Ricci tensor is 12 at  $x = 0$  and reaches 49.37738 at  $x = 1$ . Using equation (65) of [27], which in our case simplifies to

$$\mathcal{K}|_{\mathcal{H}} = 6\mathcal{R}_{AB}\mathcal{R}^{AB} - 4\Lambda\mathcal{R} + \frac{28}{9}\Lambda^2, \quad (2.11)$$

we give in Fig. 6(b) the Kretschmann scalar of the 5-dimensional space-time calculated on the horizon. The Kretschmann scalar at  $x = 0$  is 40, and it increases to 700.3672 at  $x = 1$ .

### 3 Finite Black Hole Metrics

After doing the optimization, we have the functional form of our metric including the sixth-order polynomials from the numerical calculation. This metric is conformally Schwarzschild with infinite mass at the infinite AdS boundary at  $x = 0$ . In the asymptotically infinite region, the five-dimensional bulk metric near the boundary has the form

$$ds^2 = dr^2 + e^{2r}\tilde{g}_{\mu\nu}(r, x)dx^\mu dx^\nu, \quad (3.1)$$

where  $r$  is the outward proper distance as one approaches the AdS boundary at infinite proper distance,  $r \sim \ln v$ , and  $x$  is not the same single coordinate used for the numerical calculation but instead denotes all the other four coordinates besides  $r$ . Using the Fefferman-Graham (FG) expansion [28, 29, 30],  $\tilde{g}_{\mu\nu}$  can be written as

$$\tilde{g}_{\mu\nu}(r, x) = g_{\mu\nu}^{(0)}(x) + e^{-2r}g_{\mu\nu}^{(2)}(x) + e^{-4r}g_{\mu\nu}^{(4)}(x) - 2e^{-4r}rh_{\mu\nu}^{(4)}(x) + e^{-4r}t_{\mu\nu}(x) + O(e^{-6r}). \quad (3.2)$$

When the bulk Einstein equation is considered as a second-order differential equation in the radial coordinate  $r$ , and when  $g_{\mu\nu}^{(0)}$  is the conformal metric on the infinite AdS boundary, the boundary conditions are the conformal metric  $g_{\mu\nu}^{(0)}$  and a traceless and divergenceless tensor  $t_{\mu\nu}(x)$ . Then  $g_{\mu\nu}^{(2)} = -\frac{1}{2}R_{\mu\nu}^{(0)}(x) + \frac{1}{12}R^{(0)}g_{\mu\nu}^{(0)}(x)$ . The terms  $g_{\mu\nu}^{(4)}(x)$  and  $h_{\mu\nu}^{(4)}(x)$  are functions of the Ricci tensor  $R_{\mu\nu}^{(0)}(x)$  of the asymptotic conformal metric  $g_{\mu\nu}^{(0)}(x)$ ; see [30] for their exact definitions. For our infinite mass black hole metric, we set  $g_{\mu\nu}^{(0)}(x) = g_{\mu\nu}^{\text{Sch}}$  for the RSII brane at  $r = \infty$ . Therefore, our conformal boundary metric is the Ricci-flat Schwarzschild metric.

Then, the only non-zero term in (3.2) before the  $O(e^{-6r})$  terms is the one including  $t_{\mu\nu}(x)$ . The metric has the asymptotic form

$$ds^2 = dr^2 + e^{2r} \left[ e^\beta \frac{dy^2}{y^4(1-y)} - 4e^\gamma(1-y)dt^2 + e^\delta \frac{1}{y^2}d\Omega^2 \right], \quad (3.3)$$

$$\beta = e^{-4r} t_r{}^r(y) + O(e^{-6r}), \quad (3.4)$$

$$\gamma = e^{-4r} t_t{}^t(y) + O(e^{-6r}), \quad (3.5)$$

$$\delta = e^{-4r} t_\theta{}^\theta(y) + O(e^{-6r}). \quad (3.6)$$

$t_r{}^r$ ,  $t_t{}^t$ , and  $t_\theta{}^\theta$  are the components of the traceless, divergenceless tensor  $t_\nu{}^\mu(y)$ , which is diagonal in our coordinate system. It can be shown that  $t_r{}^r$ ,  $t_t{}^t$  and  $t_\theta{}^\theta$  are the vacuum expectation values of the stress tensor components on the boundary of the CFT energy-momentum tensor,  $\langle T_r{}^r \rangle$ ,  $\langle T_t{}^t \rangle$ , and  $\langle T_\theta{}^\theta \rangle = \langle T_\varphi{}^\varphi \rangle$  respectively. We derive approximations for  $t_r{}^r$ ,  $t_t{}^t$ , and  $t_\theta{}^\theta$  as functions of  $y$  from our numerical result for the sixth-order polynomials. For finding the energy-momentum tensors as functions of  $y$ , we use the coefficients of the first and second orders of  $x$  in  $A(x, y)$ ,  $B(x, y)$ ,  $C(x, y)$ , and  $D(x, y)$ , which are functions of  $y$ . We call them  $A1(y)$ ,  $B1(y)$ ,  $C1(y)$ , and  $D1(y)$  for the coefficients of  $x$  and  $A2(y)$ ,  $B2(y)$ ,  $C2(y)$ , and  $D2(y)$  for the coefficients of  $x^2$ . Then, we calculate  $t_r{}^r$ ,  $t_t{}^t$ , and  $t_\theta{}^\theta$  by using these functions with the following formulas:

$$t_r{}^r(y) = -\frac{1}{16}y^4 \left[ 11 - 14y - (10 - 14y - 3A1)A1 - 4A2 - 16B2 - (12y - 13y^2)\frac{dA1}{dy} - 2(y^2 - y^3)\frac{d^2A1}{dy^2} \right], \quad (3.7)$$

$$t_t{}^t(y) = -\frac{1}{16}y^4 \left[ -1 - 2y + 2(1 + y + 3A1)A1 - 4A2 - 16C2 + y^2\frac{dA1}{dy} \right], \quad (3.8)$$

$$t_\theta{}^\theta(y) = \frac{1}{16}y^4 \left[ 5 - 4y - (6 - 4y + 3A1)A1 + 4A2 - 16D1 + 16D2 - 2(y - y^2)\frac{dA1}{dy} \right]. \quad (3.9)$$

Plugging back the functions  $A1(y)$ ,  $B1(y)$ ,  $C1(y)$ , and  $D1(y)$  and  $A2(y)$ ,  $B2(y)$ ,  $C2(y)$ , and  $D2(y)$  from our numerical results into the equations for  $t_r{}^r$ ,  $t_t{}^t$ , and  $t_\theta{}^\theta$ , (3.7)-(3.9) gives us

$$t_r{}^r(y) = -0.01174y^4 + 0.38148y^5 - 0.85298y^6 + 1.36570y^7 - 2.01560y^8 + 1.91160y^9 - 0.80470y^{10} + 0.08460y^{11} - 0.00739y^{12} + 0.00496y^{13} - 0.00181y^{14} + 0.00023y^{15} - 0.00001y^{16}, \quad (3.10)$$

$$t_t{}^t(y) = +0.00341y^4 + 0.48856y^5 - 1.18280y^6 + 1.10450y^7 - 0.03021y^8 - 0.65406y^9 + 0.36864y^{10} - 0.03968y^{11} - 0.00739y^{12} + 0.00496y^{13} - 0.00181y^{14} + 0.00023y^{15} - 0.00001y^{16}, \quad (3.11)$$

$$t_\theta{}^\theta(y) = +0.00261y^4 - 0.40736y^5 + 0.86236y^6 - 0.78244y^7 + .28004y^8 + 0.02035y^9 - 0.03666y^{10} + 0.01027y^{11} - 0.00739y^{12} + 0.00496y^{13} - 0.00181y^{14} + 0.00023y^{15} - 0.00001y^{16}. \quad (3.12)$$

The constraints on  $t_r{}^r$ ,  $t_t{}^t$ , and  $t_\theta{}^\theta$  as the components of a traceless conserved stress-energy tensor are

$$t_r{}^r + t_t{}^t + 2t_\theta{}^\theta = 0, \quad (3.13)$$

$$2y(1-y)\frac{d}{dy}(t_r{}^r) + y(t_t{}^t - t_r{}^r) + 4(1-y)(t_\theta{}^\theta - t_r{}^r) = 0. \quad (3.14)$$

Equation (3.13) is the traceless condition for the energy-momentum tensor,  $t_\mu{}^\mu = 0$ , and equation (3.14) corresponds to  $\nabla_\mu t^{\mu\nu} = 0$ . Checking our numerical results for the energy-momentum conditions, (3.13) and (3.14), shows small deviations from zero, which can be explained as numerical error. For the traceless condition, the maximum deviation is  $4.57 \times 10^{-4}$ , and for the  $\nabla_\mu t^{\mu\nu} = 0$  condition, it is  $1.82 \times 10^{-3}$ .

Now, we have the infinite mass black hole metric (3.3), numerically. To find the large but finite mass black hole, we need to perturb our infinite mass metric by replacing the RSII brane at the AdS conformal boundary,  $r = \infty$ , with a brane at finite  $r = -\ln \epsilon$  for  $\epsilon = e^{-r} \ll 1$ . The conformal metric  $g_{\mu\nu}^{(0)}(x)$  is perturbed to

$$g_{\mu\nu}^{(0)} = g_{\mu\nu}^{\text{Sch}} + \epsilon^2 h_{\mu\nu}, \quad (3.15)$$

with the perturbation metric  $h_{\mu\nu}$ . For the metric (3.15), the Ricci tensor is not zero, and the same is true for the  $e^{-2r}$  term in the FG expansion. The perturbation would effect the form of  $t^{\mu\nu}(x)$  as well. However, because it is multiplied by  $e^{-4r}$  in the FG expansion, and we are working to lowest non-trivial order in  $\epsilon^2$ , we can still use the values of  $t^{\mu\nu}(x)$  from the infinite mass black hole bulk solution.

The second fundamental form is  $K_{\mu\nu} = -\frac{1}{2}\partial_r[e^{2r}\tilde{g}_{\mu\nu}(r, x)]$ , where we are using the opposite sign convention from FW, so that our second fundamental form is half the positive derivative with respect to distance from the brane of the induced metric on the four-dimensional hypersurfaces at each constant distance, with the derivative evaluated at zero distance from the brane. Therefore, to first order in  $\epsilon^2$ , the Israel junction condition gives

$$g_{\mu\nu}^{(2)} = -\frac{1}{2}R_{\mu\nu}^{(0)} + \frac{1}{12}R^{(0)}(x)g_{\mu\nu}^{(0)} = -2\epsilon^2 t_{\mu\nu}. \quad (3.16)$$

As mentioned, up to this order  $t^{\mu\nu}$  is traceless. Then the Ricci tensor for the metric (3.15) is calculated as

$$R_{\mu\nu}^{(0)} = 4\epsilon^2 t_{\mu\nu}. \quad (3.17)$$

Using equation (3.17) with  $t_\mu{}^\nu(y)$  calculated from the infinite metric leads us to have the  $h_{\mu\nu}$  and spherically symmetric static metric  $g_{\mu\nu}^{(0)}$  in (3.15). The induced metric on the brane can be found as

$$\gamma_{\mu\nu} = \frac{1}{\epsilon^2}\tilde{g}_{\mu\nu} = \frac{1}{\epsilon^2}g_{\mu\nu}^{\text{Sch}} + h_{\mu\nu} + O(\epsilon^2). \quad (3.18)$$

The bulk Einstein equation plus the Israel junction condition on the brane without matter imply that the Ricci scalar for the metric on the brane is zero. To first order in  $1/R_0^2 = \epsilon^2 = (3/2)/(-\Lambda M^2)$ , the metric on the brane is

$$ds^2 = (R_0^2 + 2b)\frac{dy^2}{y^4(1-y)} - (R_0^2 + 2c)4(1-y)dt^2 + (R_0^2 + 2d)\frac{1}{y^2}d\Omega^2. \quad (3.19)$$

For a general metric on the brane, working in the gauge  $h_t^t = 0$ , we have

$$h_y^y(y) = 2b(y) = -\frac{2y^2(1-y)}{3(4-3y)}\left(F + y\frac{dF}{dy}\right), \quad (3.20)$$

$$h_t^t(y) = 2c(y) = 0, \quad (3.21)$$

$$h_\theta^\theta(y) = h_\phi^\phi(y) = 2d(y) = \frac{y^2}{6}F(y), \quad (3.22)$$

with

$$F(y) = \frac{2 - 3y}{(4 - 3y)^2} \int_0^y \frac{(4 - 3u)t_r{}^r(u)}{u^3(2 - 3u)^2} du. \quad (3.23)$$

According to (3.23), using  $t_r{}^r$  from the numerical result leads us to find  $F(y)$  and the  $h_{\mu\nu}$  components afterwards.

It can be shown that the asymptotic behaviour of  $t_{\mu\nu}$  goes as  $y^5$ , and we know that  $t_{\mu\nu}$  is traceless. Considering the above characteristics for  $t_{\mu\nu}$ , we try to find the traceless conserved fits for  $t_r{}^r$ ,  $t_t{}^t$ , and  $t_\theta{}^\theta$  back in (3.23). We define  $F(y)$  as a polynomial with unknown coefficients, and define  $\hat{t}_r{}^r$ ,  $\hat{t}_t{}^t$ , and  $\hat{t}_\theta{}^\theta$  as follows:

$$\hat{t}_r{}^r(y) = \frac{y^5}{12(4 - 3y)} \left[ 6(1 - y)F + y(2 - 3y) \frac{dF}{dy} \right], \quad (3.24)$$

$$\hat{t}_\theta{}^\theta(y) = -2\hat{t}_r{}^r(y) + \hat{\epsilon}(y), \quad (3.25)$$

$$\hat{t}_t{}^t(y) = 3\hat{t}_r{}^r(y) - 2\hat{\epsilon}(y), \quad (3.26)$$

$$\hat{\epsilon}(y) = \frac{y^5}{12(4 - 3y)^2} \left[ 12(1 - y^2)F - y(12 - 14y + 3y^2) \frac{dF}{dy} - y^2(1 - y)(4 - 3y) \frac{d^2F}{dy^2} \right], \quad (3.27)$$

where finding fits for our numerical energy-momentum tensor components as functions of  $y$  will help us to compare our results with the FLW results in the next section.

#### 4 RSII black hole metric on the brane

We can now write the metric on the brane in terms of the function  $F$ . Define  $(2M)^2 \equiv 1/\epsilon^2 = 6/(-\Lambda\epsilon^2)$  and the new radial coordinate  $\rho = 2M/y$ . Then, to first order in  $\epsilon^2 = (3/2)/(-\Lambda M^2)$ , the metric on the brane reads

$$\begin{aligned} {}^4ds^2 = \gamma_{\mu\nu} dx^\mu dx^\nu = & \left[ 1 - \frac{1}{(-\Lambda\rho^2)} \frac{\rho - 2M}{\rho - 1.5M} \left( F - \rho \frac{dF}{d\rho} \right) \right] \left( 1 - \frac{2M}{\rho} \right)^{-1} d\rho^2 \\ & - \left( 1 - \frac{2M}{\rho} \right) dt^2 + \left[ \rho^2 + \frac{1}{(-\Lambda)} F \right] d\Omega^2, \end{aligned} \quad (4.1)$$

where we have rescaled the time coordinate  $t$  by a factor of  $4M$  so that  $\gamma_{tt} = -1$  at  $\rho = \infty$ .

One can show that to have the leading order of the Einstein equation for the five-dimensional infinite black hole metric (2.4) satisfied at the corner  $x = 0$  and  $\rho \rightarrow \infty$ , the asymptotic behavior of  $\beta$ ,  $\gamma$ , and  $\delta$  must be as  $1/\rho^5$  for  $\rho \gg 2M$ . This is in accordance to the result of Figueras and Wiseman [23] and [24], that  $t_{\mu\nu}$  goes as  $1/\rho^5$ . This asymptotic behavior of  $t_{\mu\nu}$  implies that  $F$  approaches unity as  $\rho \rightarrow \infty$ . To fit to our data  $t_{\mu\nu}^{(2)}(x) = t_{\mu\nu}^{\text{our}}(x)$ , and to fit to the FLW data, which they have kindly sent us,  $t_{\mu\nu}^{(1)}(x) = t_{\mu\nu}^{\text{FLW}}(x)$ , we took  $F_1 = F_{\text{FLW}}$  and  $F_2 = F_{\text{our}}$  to be cubic polynomials in  $y \equiv 2M/\rho$  with the constant coefficient set to unity, and  $F_{11}$  to be an 11th order polynomial with the constant coefficient set to unity and then chose the other coefficients in each case to minimize the respective

$$J_i = \frac{\int \rho^4 \Delta t_{\mu\nu}^{(i)} \Delta t_{\mu\nu}^{\mu\nu} \sqrt{-{}^{(4)}\gamma} d^4x}{\int \rho^4 t_{\mu\nu}^{\text{FLW}} t_{\mu\nu}^{\text{FLW}} \sqrt{-{}^{(4)}\gamma} d^4x}. \quad (4.2)$$

For the two values of  $i$  ( $i = 1$  for the FLW data and  $i = 2$  for our data), in the numerator

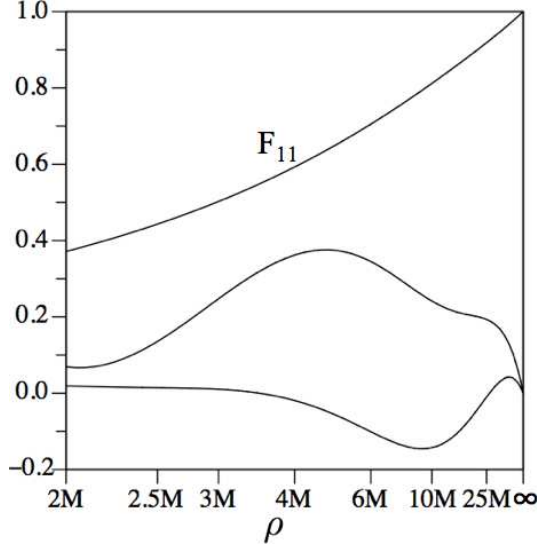


**Figure 7.** At the top is an 11th-order polynomial fit  $F_{11}$  to the FLW data, which gave normalized mean-square error  $J_{11} = 0.0000572$ , 92% of  $J_{\text{FLW}}$ . Because the differences from  $F_{11}$  of the cubic fits  $F_{\text{FLW}}$  and  $F_{\text{our}}$  are too small to show up when plotted directly on this graph, at the bottom we have expanded these differences by a factor of 50 and plotted  $50(F_{\text{FLW}} - F_{11})$  (bottom curve) and  $50(F_{\text{our}} - F_{11})$  (middle curve).

$\Delta t_{\mu\nu}^{(i)} = t_{\mu\nu}^{F_i} - t_{\mu\nu}^{(i)}$  is the difference between the  $t_{\mu\nu}^{F_i}(x)$  given by the cubic for  $F_i(x)$  and the  $t_{\mu\nu}^{(i)}$  given by the numerical data. To find the 11th order polynomial fit to the FLW data,  $\Delta t_{\mu\nu}^{11} = t_{\mu\nu}^{F_{11}} - t_{\mu\nu}^{\text{FLW}}$ , the difference between the  $t_{\mu\nu}^{F_{11}}(x)$  given by the 11th order fit  $F_{11}$  and the  $t_{\mu\nu}^{\text{FLW}}$  given by the FLW numerical data. The integral in the denominator was included to make  $J$  a normalized mean-square error. It has  $t_{\mu\nu}^{\text{FLW}}(x)$  given by the FLW numerical data, the same in each case to give a constant normalizing factor. The factor of  $\rho^4$  was included to increase the weight of the large- $\rho$  part, though the integrals are still dominated by the small- $\rho$  part, since  $t_{\mu\nu}(x)$  drops off asymptotically as the inverse fifth power of the radial coordinate  $\rho$  [23, 24]. For small  $1/(-\Lambda M^2)$ , Eq. (4.2) is approximately equivalent to

$$J_i = \frac{\int \rho^6 \Delta t_{\mu\nu}^{(i)} \Delta t_{\mu\nu}^{(i)} d\rho}{\int \rho^6 t_{\mu\nu}^{\text{FLW}} t_{\mu\nu}^{\text{FLW}} d\rho}. \quad (4.3)$$

We minimize (4.3), finding the coefficients of  $F_1 = F_{\text{FLW}}$  and  $F_2 = F_{\text{our}}$ . For the FLW numerical data  $t_{\mu\nu}^{\text{FLW}}(x)$ ,  $J_1$  was minimized at  $J_{\text{FLW}} \approx 0.0000620$  with

$$F_{\text{FLW}} \approx 1 - 1.062 \left( \frac{2M}{\rho} \right) + 0.554 \left( \frac{2M}{\rho} \right)^2 - 0.120 \left( \frac{2M}{\rho} \right)^3. \quad (4.4)$$

For our numerical data  $t_{\mu\nu}^{\text{our}}(x)$ , the normalized mean-square error  $J_2$  was minimized at  $J_{\text{our}} \approx 0.00139$  for

$$F_{\text{our}} \approx 1 - 1.002 \left( \frac{2M}{\rho} \right) + 0.434 \left( \frac{2M}{\rho} \right)^2 - 0.059 \left( \frac{2M}{\rho} \right)^3. \quad (4.5)$$

Our data is less accurate than the FLW data, giving  $J_{\text{our}} \approx 22J_{\text{FLW}}$ . This is not unexpected, since we varied only 210 parameters in our spectral method, whereas FLW used

	$t_{\mu\nu}^{F_{11}}$	$t_{\mu\nu}^{F_{\text{FLW}}}$	$t_{\mu\nu}^{F_{\text{our}}}$
$t_{\mu\nu}^{\text{FLW}}$	$J_{11} \approx 0.0000572$	$J_{\text{FLW}} \approx 0.0000620$	$J_7 \approx 0.000214$
$t_{\mu\nu}^{F_{11}}$	0	$J_5 \approx 0.000004793$	$J_6 \approx 0.000156$
$t_{\mu\nu}^{F_{\text{FLW}}}$	$J_5 \approx 0.000004793$	0	$J_4 \approx 0.000146$

**Table 2.** Values of  $J_i$  from Eq (4.2), with  $\Delta t_{\mu\nu}^{(i)}$  calculated as difference between the column  $t_{\mu\nu}$  and the row  $t_{\mu\nu}$ .

grids of  $40 \times 40$  (or 1600 points) and of  $160 \times 160$  (or 25600 points). Also, the individual coefficients of these two cubics have large relative differences, but the ratio of the two cubics themselves never differs by more than 1.3% from unity, so they show good agreement between what is generated by our numerical data and by what is given by the FLW data.

We then found an 11th-order polynomial  $F_{11}$  to the FLW data, which gave normalized mean-square error  $J_{11} \approx 0.0000572$  for

$$\begin{aligned}
F_{11} = & 1 - 1.1241 \left(\frac{2M}{\rho}\right) + 1.956 \left(\frac{2M}{\rho}\right)^2 - 9.961 \left(\frac{2M}{\rho}\right)^3 + 35.475 \left(\frac{2M}{\rho}\right)^4 \\
& - 75.962 \left(\frac{2M}{\rho}\right)^5 + 99.432 \left(\frac{2M}{\rho}\right)^6 - 73.694 \left(\frac{2M}{\rho}\right)^7 + 18.726 \left(\frac{2M}{\rho}\right)^8 \\
& + 13.990 \left(\frac{2M}{\rho}\right)^9 - 12.366 \left(\frac{2M}{\rho}\right)^{10} + 2.900 \left(\frac{2M}{\rho}\right)^{11}. \tag{4.6}
\end{aligned}$$

We have compared  $F_{11}$ ,  $F_{\text{our}}$ , and  $F_{\text{FLW}}$  in Fig 7. Using  $F_{\text{our}}$ ,  $F_{\text{FLW}}$ , and  $F_{11}$ , we can derive the corresponding  $t_{\mu\nu}^{F_{11}}$  derived from the 11th order fit  $F_{11}$  to the FLW data,  $t_{\mu\nu}^{F_{\text{FLW}}}$  derived from the cubic fit  $F_{\text{FLW}}$  to the FLW data, and  $t_{\mu\nu}^{F_{\text{our}}}$  derived from the cubic fit  $F_{\text{our}}$  to our data. In part (a) of Figs. 8, 9, and 10 we have considered the ratios of each of the three individual components of the three versions of  $t_{\mu}^{\nu F_i}$  ( $i = 1$  for  $F_{\text{FLW}}$ ,  $i = 2$  for  $F_{\text{our}}$  and  $i = 11$  for  $F_{11}$ ) to  $t_{\mu}^{\nu FLW}$ . These ratios were generally within 1 – 2% of unity, with the maximum differing by less than 2.9%.

In part (b) of Figs. 8, 9, and 10 we have compared the difference between individual components of  $t_{\mu}^{\nu F_{\text{our}}}$  with  $t_{\mu}^{\nu F_{11}}$  and  $t_{\mu}^{\nu F_{\text{FLW}}}$  with  $t_{\mu}^{\nu F_{11}}$ . The ratios of each of the three components of  $t_{\mu\nu}^{F_{\text{our}}}$  to  $t_{\mu\nu}^{F_{\text{FLW}}}$  as given in Fig 11 (a) is within 2.8% of unity. The mean-square error between the  $t_{\mu\nu}^{F_{\text{our}}}(x)$  generated by our  $F_{\text{our}}$  fit to our data and the  $t_{\mu\nu}^{F_{\text{FLW}}}(x)$  generated by the  $F_{\text{FLW}}$  fit to the FLW data, using in Eq. (4.3)  $\Delta t_{\mu\nu}^{(4)} = t_{\mu\nu}^{F_{\text{our}}} - t_{\mu\nu}^{F_{\text{FLW}}}(x)$ , is  $J_4 = J_{\text{our fit vs. FLW fit}} \approx 0.000146 \approx 2.4 J_{\text{FLW}}$ . Thus, the  $t_{\mu\nu}^{F_{\text{our}}}(x)$  generated by our  $F_{\text{our}}$  fits the  $t_{\mu\nu}^{F_{\text{FLW}}}(x)$  generated by the  $F_{\text{FLW}}$  fit to the FLW data nearly 9 times better than it fits the  $t_{\mu\nu}^{\text{our}}(x)$  directly extracted from our data, which is not quite traceless and conserved, as the  $t_{\mu\nu}^{F_{\text{our}}}(x)$  generated by the fitting  $F_{\text{our}}$  is constrained to be.

We also calculated  $J_5 = J_{F_{11} \text{ fit vs. FLW fit}} \approx 0.000004793$ , where now in Eq. (4.3)  $\Delta t_{\mu\nu}^{(5)} = t_{\mu\nu}^{F_{11}} - t_{\mu\nu}^{F_{\text{FLW}}}(x)$ . Furthermore, we calculated  $J_6 = J_{F_{11} \text{ fit vs. our } F_{\text{our}} \text{ fit}} \approx 0.000156$ , where  $\Delta t_{\mu\nu}^{(6)} = t_{\mu\nu}^{F_{11}} - t_{\mu\nu}^{F_{\text{our}}}(x)$ . The mean-square error between the  $t_{\mu\nu}^{F_{\text{our}}}(x)$  generated by our  $F_{\text{our}}$  fit to our data and the FLW data,  $t_{\mu\nu}^{FLW}(x)$ , using in Eq. (4.3)  $\Delta t_{\mu\nu}^{(4)} = t_{\mu\nu}^{F_{\text{our}}} - t_{\mu\nu}^{FLW}(x)$ , is  $J_7 = J_{\text{our fit vs. FLW data}} \approx 0.000214$ . For the summary of the comparison between different  $t_{\mu\nu}$ 's, refer to Table 2.

Let us consider the trace of the square of energy momentum tensor,  $\mathcal{T} = t_\nu^\mu t_\mu^\nu = (t_t^t)^2 + (t_\rho^\rho)^2 + 2(t_\phi^\phi)^2$ . We have plotted  $\mathcal{T}^{F_{11}}$  derived from  $t_\mu^{\nu F_{11}}$ 's in Fig 11 (b). We made comparison between  $\mathcal{T}^{F_i}$ 's and  $\mathcal{T}^{FLW}$  which is directly given by the FLW data, Fig. 12 (a). The  $\mathcal{T}^{F_i}$ 's and  $\mathcal{T}^{FLW}$  are in agreement within 3.9%. In addition from Fig 12 (b) the  $\mathcal{T}^{F_i}$  and  $\mathcal{T}^{F_j}$  are in agreement within 4%.

We have calculated  $h_y^y$  from  $F_{11}$ ,  $F_{FLW}$ , and  $F_{our}$  using Eq. (3.20), where  $h_y^y$  generated from  $F_{11}$  is shown in Fig. 13(a). The ratio of the  $h_y^y$  generated by  $F_{our}$  to  $F_{FLW}$ , which involves a derivative of  $F$  as given in Eq. (3.20), differ by up to about 9.3%, as shown in Fig. 13(b), while the ratio of the  $h_\theta^\theta = h_\phi^\phi$ , generated by using Eq. (3.22),  $F_{our}$ , and  $F_{FLW}$  agree with unity to a very good precision of 1.3%, as shown in Fig. 14(b).

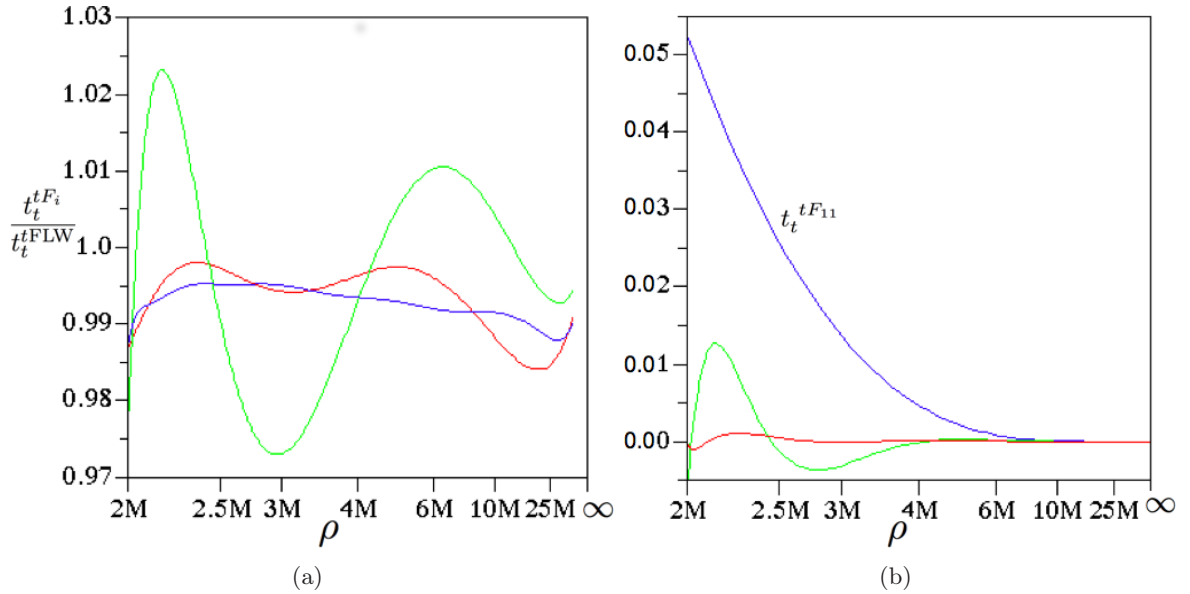


**Figure 8.** (a) The blue line is the ratio of the  $t_t^{F_{11}}$ , derived from the 11th-order polynomial fit  $F_{11}$  to the FLW data, to  $t_t^{FLW}$ , vs.  $\rho$ . The red line is the ratio of the  $t_t^{F_{FLW}}$ , derived from the cubic fit  $F_{FLW}$  to the FLW data, to  $t_t^{FLW}$ . The green line is the ratio of the  $t_t^{F_{our}}$ , derived from the cubic fit  $F_{our}$  to our data, to  $t_t^{FLW}$ . (b) The blue line is the  $t_t^{F_{11}}$ . The red line is the difference between the  $t_t^{F_{FLW}}$ , derived from the cubic fit  $F_{FLW}$  to the FLW data, and the  $t_t^{F_{11}}$ , derived from the 11th order fit to the FLW data, times 10, i.e.,  $10(t_t^{FLW} - t_t^{F_{11}})$ . The green line is the difference between the  $t_t^{F_{our}}$ , derived from the cubic fit to our data, and the  $t_t^{F_{11}}$ , derived from the 11th order fit to the FLW data, multiplied by 10, i.e.,  $10(t_t^{our} - t_t^{F_{11}})$ .

Having found  $F$ 's up to a good accuracy for both our numerical data and the FLW data, we can calculate some of the parameters of a RSII black hole on the brane as given by the metric (4.1). The ADM mass, temperature, entropy and area of the RSII black hole on the brane, up to first order in  $1/(-\Lambda M^2)$ , are

$$T = \frac{1}{8\pi M} + O\left(\frac{1}{\Lambda^2 M^5} \ln(-\Lambda M^2)\right), \quad (4.7)$$

$$S = 4\pi M^2 + \text{const} + O\left(\frac{1}{\Lambda^2 M^2} \ln(-\Lambda M^2)\right), \quad (4.8)$$

$$A = 16\pi M^2 + \frac{4\pi}{-\Lambda} F(1) + O\left(\frac{1}{\Lambda^2 M^2} \ln(-\Lambda M^2)\right). \quad (4.9)$$



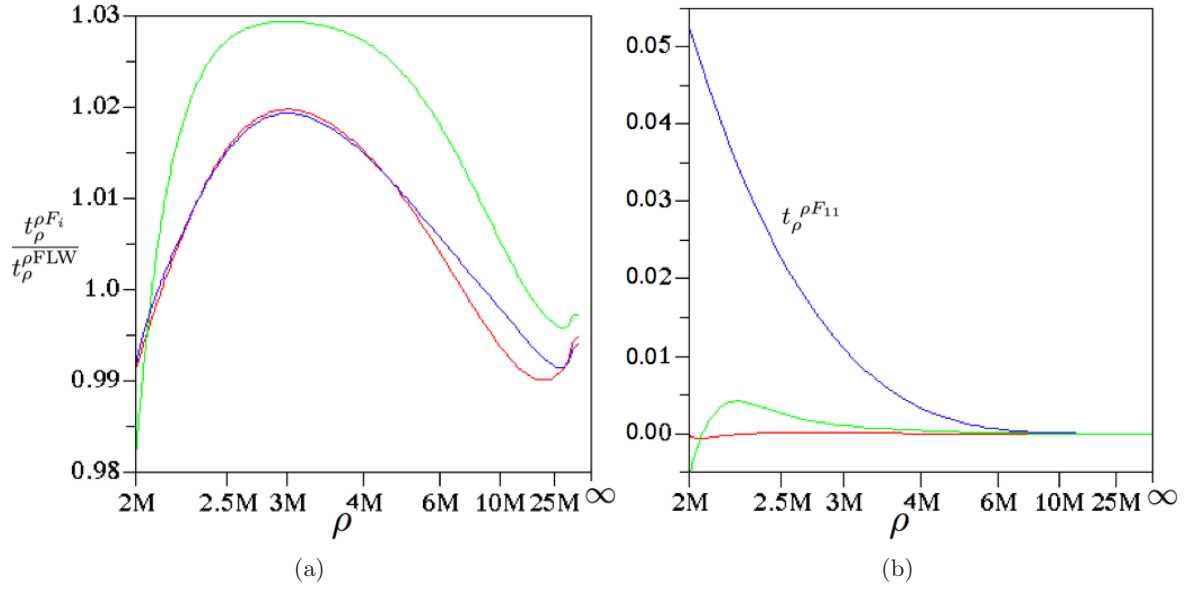


**Figure 9.** (a) The blue line is the ratio of the  $t_\rho^{\rho F_{11}}$ , derived from the 11th-order polynomial fit  $F_{11}$  to the FLW data, to  $t_\rho^{\rho FLW}$ . The red line is the ratio of the  $t_\rho^{\rho F_{FLW}}$ , derived from the cubic fit  $F_{FLW}$  to the FLW data, to  $t_\rho^{\rho FLW}$ . The green line is the ratio of the  $t_\rho^{\rho F_{our}}$ , derived from the cubic fit  $F_{our}$  to our data, to  $t_\rho^{\rho FLW}$ . (b) The blue line is the  $t_\rho^{\rho F_{11}}$ . The red line is 10 times the difference between the  $t_\rho^{\rho F_{FLW}}$ , derived from the cubic fit  $F_{FLW}$  to the FLW data, and the  $t_\rho^{\rho F_{11}}$ , derived from the 11th order fit to FLW data, i.e.,  $10(t_\rho^{\rho F_{FLW}} - t_\rho^{\rho F_{11}})$ . The green line is  $10(t_\rho^{\rho F_{our}} - t_\rho^{\rho F_{11}})$ .

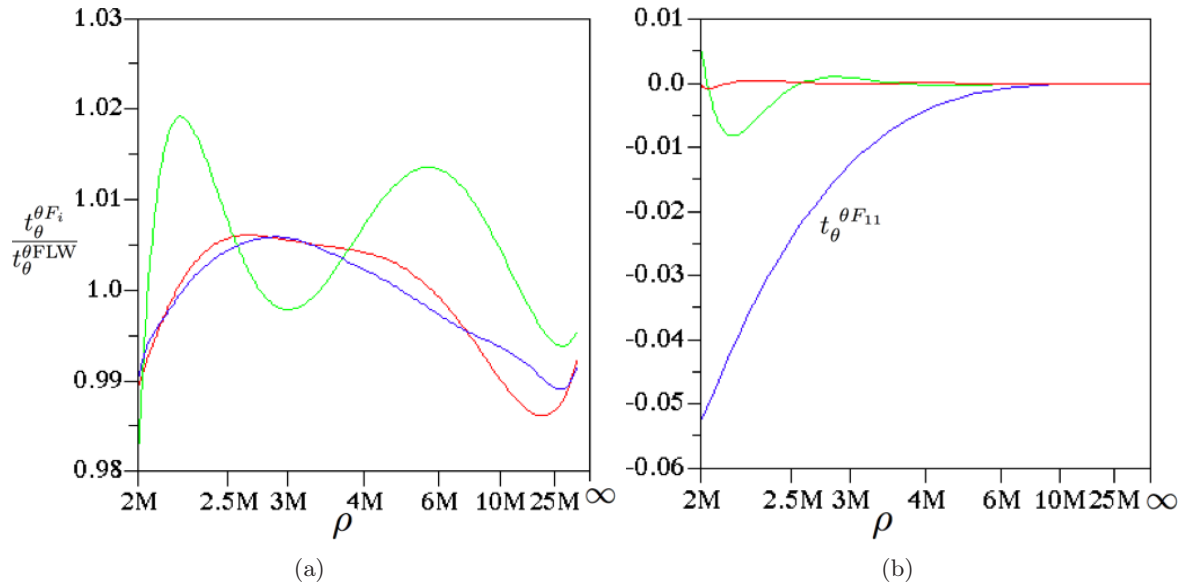


**Figure 10.** (a) The blue, red, and green lines are the ratio of  $t_\theta^{\theta F_{11}}$ ,  $t_\theta^{\theta F_{FLW}}$ , and  $t_\theta^{\theta F_{our}}$  to the FLW data  $t_\theta^{\theta FLW}$ , respectively. (b) The blue line is the  $t_\theta^{\theta F_{11}}$ . The red and green lines are 10 times the difference of  $t_\theta^{\theta F_{FLW}}$  and  $t_\theta^{\theta F_{our}}$  with  $t_\theta^{\theta F_{11}}$ , respectively.

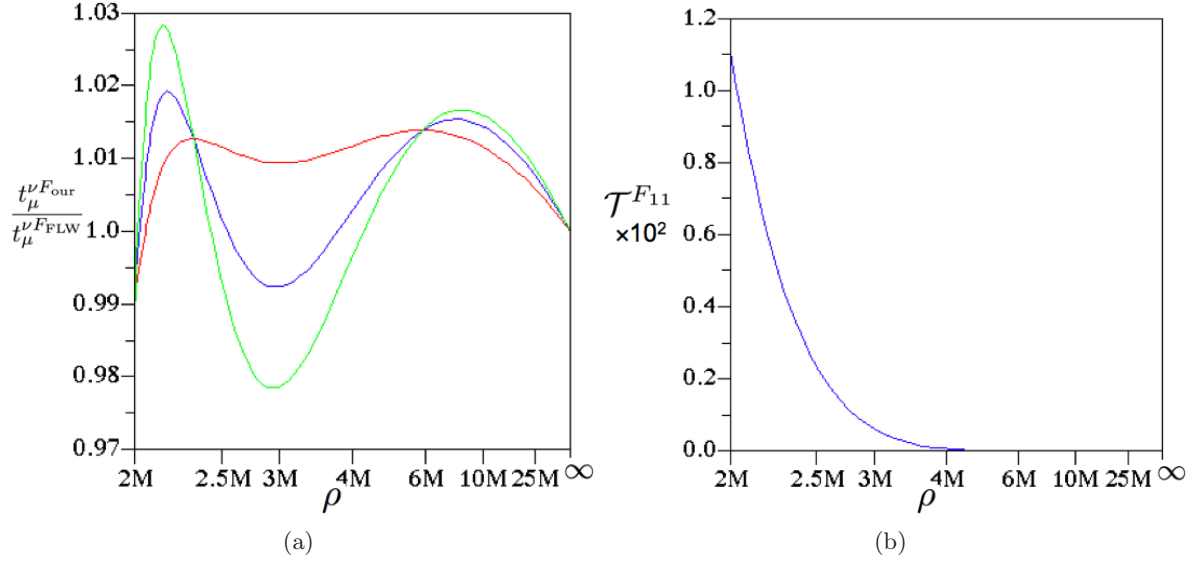


**Figure 11.** (a) The green, red, and blue lines are the ratios of  $t_t^{tF_{\text{our}}}$ ,  $t_\rho^{\rho F_{\text{our}}}$ , and  $t_\theta^{\theta F_{\text{our}}}$  to the corresponding  $t_i^{jF_{\text{FLW}}}$ . (b)  $\mathcal{T}^{F_{11}} = t_{\mu\nu}^{F_{11}} t_{F_{11}}^{\mu\nu}$ .

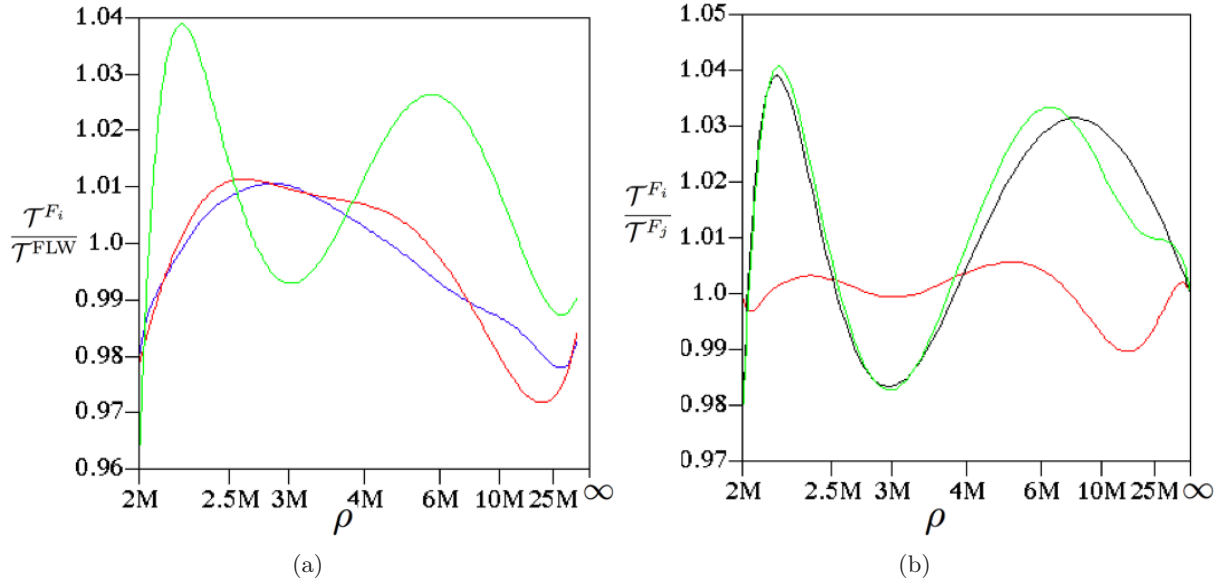


**Figure 12.** (a) The blue, red, and green lines are the ratios of  $\mathcal{T}^{F_{11}}$ ,  $\mathcal{T}^{F_{\text{FLW}}}$ , and  $\mathcal{T}^{F_{\text{our}}}$  to  $\mathcal{T}^{F_{\text{FLW}}}$ . (b) The violet, red, and green lines are the ratios  $\mathcal{T}^{F_{\text{our}}}/\mathcal{T}^{F_{\text{FLW}}}$ ,  $\mathcal{T}^{F_{\text{our}}}/\mathcal{T}^{F_{11}}$ , and  $\mathcal{T}^{F_{11}}/\mathcal{T}^{F_{\text{FLW}}}$ , respectively.

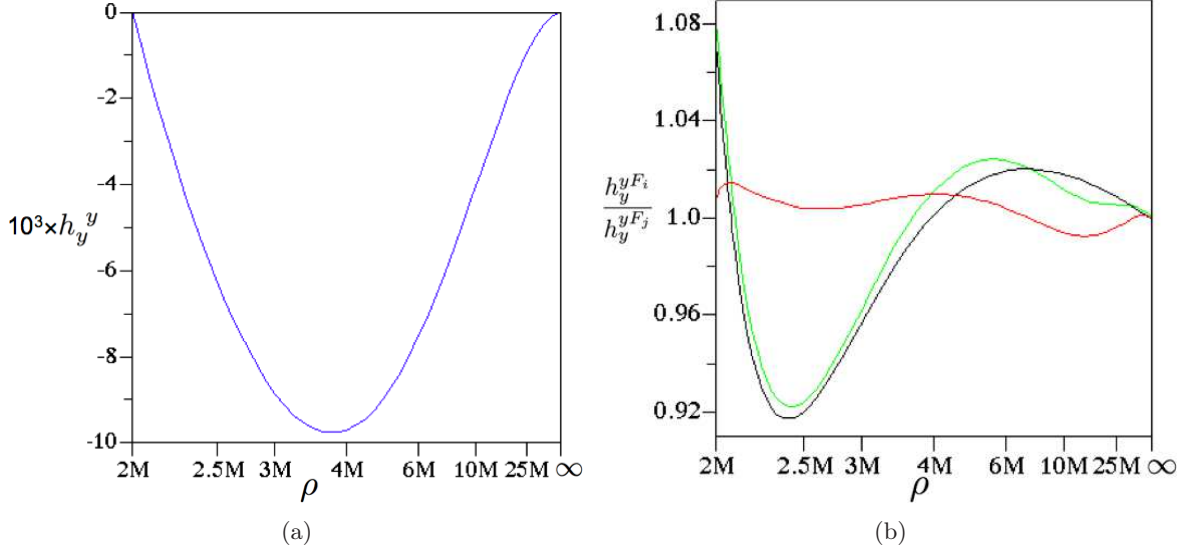


**Figure 13.** (a)  $h_y^{yF_{11}}$ . (b) The violet, red, and green lines are the ratios  $h_y^{yF_{\text{our}}}/h_y^{yF_{\text{FLW}}}$ ,  $h_y^{yF_{\text{our}}}/h_y^{yF_{11}}$ , and  $h_y^{yF_{\text{FLW}}}/h_y^{yF_{11}}$ , respectively.

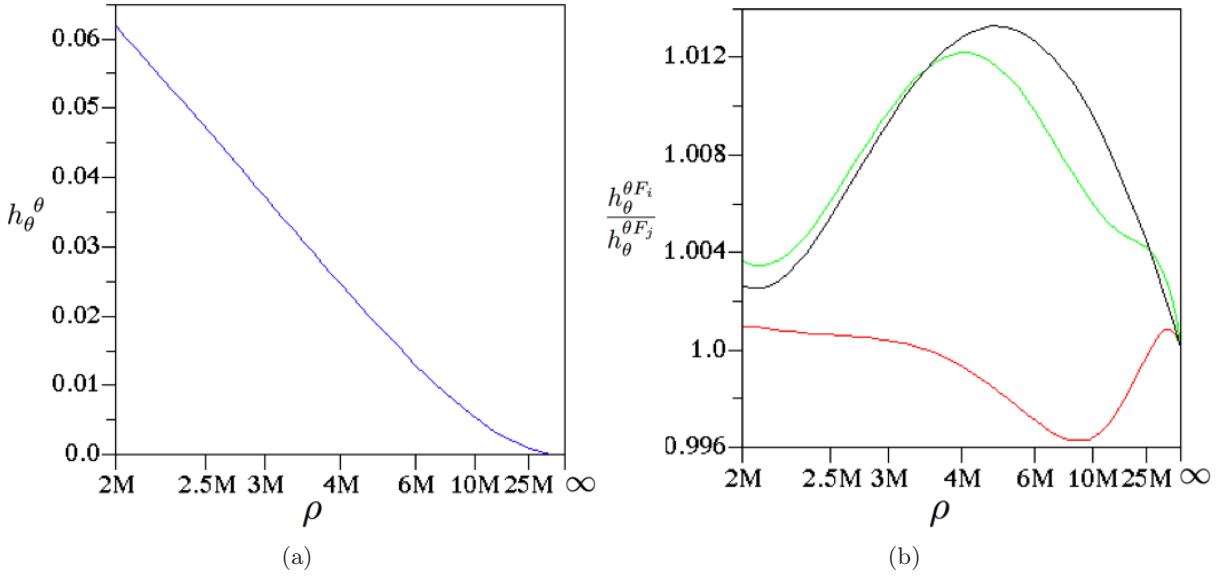


**Figure 14.** (a)  $h_\theta^{\theta F_{11}}$ . (b) The violet, red, and green lines are the ratios  $h_\theta^{\theta F_{\text{our}}}/h_\theta^{\theta F_{\text{FLW}}}$ ,  $h_\theta^{\theta F_{\text{our}}}/h_\theta^{\theta F_{11}}$ , and  $h_\theta^{\theta F_{\text{FLW}}}/h_\theta^{\theta F_{11}}$ , respectively.

For any  $F$  that has only a constant term and negative powers of  $\rho$ , such as  $F_{\text{FLW}}$  given by Eq. (4.4),  $F_{\text{our}}$  given by Eq. (4.5), and  $F_{11}$  given by Eq. (4.6), the ADM mass is precisely  $M$  and the surface gravity of the black hole is  $1/(4M)$ . Aside from the numerical approximations for determining  $F$ , the metric (4.1) is only correct to first order in our perturbation parameter  $1/(-\Lambda M^2)$ , so there might be corrections to the surface gravity of a static RSII black hole to second order in  $1/(-\Lambda M^2)$ . However, one can deduce that to first order in  $1/(-\Lambda M^2)$ , the Hawking temperature and entropy for the RSII black hole have the same values as they do for the Schwarzschild metric.

On the other hand, the horizon area is shifted from the Schwarzschild value  $A_{\text{Sch}} = 4\pi(2M)^2$  to  $A_{\text{RSII}} = 4\pi[(2M)^2 + F(1)/(-\Lambda)]$ , where  $F(1)$  is the value of  $F$  on the horizon, at  $y \equiv 2M/\rho = 1$ . For the fit to the FLW data,  $F_{\text{FLW}}(1) \approx 0.372$ , which gives the area change  $\Delta A = 4\pi F(1)/(-\Lambda) \approx 4.67/(-\Lambda)$ , as compared to the Schwarzschild black hole with the same ADM mass  $M$ . For the fit to the FLW data with the 11th order polynomial  $F_{11}(1)$  is also  $\approx 0.372$ . For the fit to our numerical data,  $F_{\text{our}}(1) \approx 0.373$ , or  $\Delta A \approx 4.69/(-\Lambda)$ , which agrees within about 0.3% with FLW fit. Therefore the RSII black hole on the brane has a larger horizon area as compared to the Schwarzschild black hole with the same ADM mass  $M$  by the amount  $\Delta A = 4\pi F(1)/(-\Lambda) \approx 4.67/(-\Lambda)$ , where here we used the FLW data value as probably more accurate.

## 5 Conclusion

We have constructed an infinite mass axisymmetric 5-dimensional black hole solution to the bulk Einstein equation with a cosmological constant  $\Lambda = -6$ . To do so, we have first expressed the metric (2.4) in terms of the polynomial functions  $A, B, C$ , and  $D$ . We then have written these polynomial functions in terms of new ones  $f, g, \tilde{A}, \tilde{B}, \tilde{C}$ , and  $\tilde{D}$ , Eq. (2.5), imposing the regularity conditions, and solving the Einstein equations to lowest order in  $x$ . Then, we have used a numerical approach, which to our knowledge is novel in the realm of general relativity, minimizing the integral of the squared error, Eq. (2.7), reducing it from 4038 for  $A = B = C = D = 1$  to  $4.2385 \times 10^{-4}$  for 6th order polynomials with 210 coefficients. We have obtained a closed-form approximation to the functions  $A, B, C$ , and  $D$ , and thus the metric (2.4).

We then have used this infinite mass 5-dimensional black hole solution to find the metric of a large Randall-Sundrum II black hole on the brane. Our result is independent numerical evidence in support of the numerical discovery of Figueras and Wiseman [23] of the existence of large static black holes in the Randall-Sundrum II braneworld model [7], by a significantly different numerical method. We have thoroughly compared our results to theirs and have shown that our results agree quite well with theirs. We have obtained a good closed-form approximation to the metric of the black hole on the brane, Eqs. (4.1) and either (4.4), (4.5), or (4.6). Our confirmation of the large black holes in RS II found by Figueras and Wiseman [23], and the fact that they are very nearly the same as Schwarzschild black holes, show that the RSII model can still be in agreement with astrophysical observations. If large black holes did not exist in the Randall-Sundrum II braneworld model, the astrophysical observations of such black holes would have been strong evidence against the viability of that model.

We have also shown the new result that to first order in our perturbation parameter  $1/(-\Lambda M^2)$ , the Hawking temperature and entropy of the black hole is the same as that of a Schwarzschild black hole of the same ADM mass  $M$ , while the RSII black hole on the brane has a larger horizon area as compared to the Schwarzschild black hole with the same ADM mass  $M$  by the amount  $\Delta A = 4\pi F(1)/(-\Lambda) \approx 4.67/(-\Lambda)$ .

## A Explicit Form of Functions

The functions  $A$ ,  $B$ ,  $C$  and  $D$  in the metric (2.4), after numerically minimizing the integral of the squared error, Eq. (2.7), by 6th order polynomials with 210 coefficients, are given by the following expressions, with all of the coefficients rounded to five digits after the decimal place:

$$\begin{aligned}
A(x, y) = & 1 + (0.21094 + 0.95771y - 0.32215y^2 + 0.07863y^3 \\
& - 0.14553y^4 + 0.08707y^5 - 0.00708y^6)x \\
& + (0.483120 - 2.96522y + 3.12221y^2 + 1.58758y^3 \\
& - 3.26594y^4 + 1.42017y^5 - 0.15995y^6)x^2 \\
& + (-1.71060 + 15.96474y - 30.20818y^2 + 13.67479y^3 \\
& + 7.52368y^4 - 6.45629y^5 + 0.54667y^6)x^3 \\
& + (5.78445 - 61.41107y + 170.77950y^2 - 214.55752y^3 \\
& + 153.70395y^4 - 73.81142y^5 + 20.14974y^6)x^4 \\
& + (-11.34737 + 143.59002y - 527.23697y^2 + 941.06600y^3 \\
& - 951.41715y^4 + 539.77303y^5 - 135.40474y^6)x^5 \\
& + (14.60367 - 212.76740y + 940.10896y^2 - 2014.17705y^3 \\
& + 2340.50264y^4 - 1423.20017y^5 + 356.46300y^6)x^6 \\
& + (-11.53285 + 191.11234y - 965.53690y^2 + 2306.98150y^3 \\
& - 2889.53569y^4 + 1827.70113y^5 - 460.15121y^6)x^7 \\
& + (5.01719 - 94.50791y + 529.64141y^2 - 1357.87635y^3 \\
& + 1776.26250y^4 - 1148.20207y^5 + 289.36969y^6)x^8 \\
& + (-0.90738 + 19.65670y - 120.15064y^2 + 323.38343y^3 \\
& - 433.62615y^4 + 282.63877y^5 - 70.80546y^6)x^9, \tag{A.1}
\end{aligned}$$

$$\begin{aligned}
B(x, y) = & 1 + (-0.60547 - 0.47885y + 0.16108y^2 - 0.03931y^3 \\
& + 0.07277y^4 - 0.04354y^5 + 0.003540y^6)x \\
& + (0.43149 - 0.80874y + 0.89420y^2 - 0.31160y^3 \\
& - 0.09760y^4 + 0.08441y^5 - 0.00482y^6)x^2 \\
& + (0.21851 + 0.08687y - 1.72664y^2 + 2.47145y^3 \\
& - 0.92513y^4 - 0.07910y^5 + 0.05733y^6)x^3 \\
& + (-0.24942 + 0.72759y + 3.13465y^2 - 9.10834y^3 \\
& + 8.03309y^4 - 3.11900y^5 + 0.42049y^6)x^4 \\
& + (0.11567 + 0.85762y - 8.90011y^2 + 22.33435y^3 \\
& - 24.96171y^4 + 13.30179y^5 - 2.72886y^6)x^5 \\
& + (0.11933 - 2.07556y + 11.88780y^2 - 30.32368y^3 \\
& + 37.81788y^4 - 22.84820y^5 + 5.46718y^6)x^6 \\
& + (-0.03621 + 0.99966y - 7.11882y^2 + 20.49026y^3 \\
& - 28.00052y^4 + 18.39565y^5 - 4.74288y^6)x^7 \\
& + (0.00555 - 0.20539y + 1.74472y^2 - 5.66200y^3 \\
& + 8.40417y^4 - 5.81216y^5 + 1.52634y^6)x^8, \tag{A.2}
\end{aligned}$$

$$\begin{aligned}
C(x, y) = & 1 + (-0.60547 - 0.47885y + 0.16108y^2 - 0.03931y^3 \\
& + 0.07277y^4 - 0.04353y^5 + 0.00354y^6)x \\
& + (-0.14516 + 1.32670y - 1.67755y^2 + 0.52746y^3 \\
& + 0.82884y^4 - 1.10767y^5 + 0.49529y^6 - 0.06057y^7)x^2 \\
& + (0.27707 - 2.97720y + 6.80878y^2 - 6.66724y^3 \\
& + 2.34156y^4 + 2.29259y^5 - 2.95084y^6 + 0.978589y^7)x^3 \\
& + (-0.54534 + 5.46359y - 13.40233y^2 + 12.20018y^3 \\
& + 3.69101y^4 - 21.56518y^5 + 20.75440y^6 - 6.75727y^7)x^4 \\
& + (0.63505 - 6.58020y + 16.26668y^2 - 7.88244y^3 \\
& - 32.05193y^4 + 69.62487y^5 - 57.58350y^6 + 17.59022y^7)x^5 \\
& + (-0.42810 + 5.02395y - 14.87309y^2 + 10.13469y^3 \\
& + 30.26574y^4 - 73.46057y^5 + 62.70428y^6 - 19.32214y^7)x^6 \\
& + (0.15406 - 2.23357y + 9.56540y^2 - 15.94279y^3 \\
& + 4.13362y^4 + 20.02335y^5 - 24.13180y^6 + 8.41885y^7)x^7 \\
& + (-0.01891 + 0.44363y - 2.86261y^2 + 7.61814y^3 \\
& - 9.31272y^4 + 4.24741y^5 + 0.75762y^6 - 0.87134y^7)x^8, \tag{A.3}
\end{aligned}$$

$$\begin{aligned}
D(x, y) = & 1 + (0.39453 - 0.47885y + 0.16108y^2 - 0.03931y^3 \\
& + 0.07276y^4 - 0.04354y^5 + 0.00354y^6)x \\
& + (0.05130 + 0.60697y - 0.17110y^2 - 1.10809y^3 \\
& + 1.02899y^4 - 0.23688y^5 - 0.02783y^6)x^2 \\
& + (0.32335 - 2.49967y + 5.37277y^2 - 6.15484y^3 \\
& + 7.81122y^4 - 7.43134y^5 + 2.80293y^6)x^3 \\
& + (-0.52530 + 7.18773y - 31.23730y^2 + 79.39889y^3 \\
& - 119.57662y^4 + 94.40212y^5 - 29.80903y^6)x^4 \\
& + (0.58030 - 12.77895y + 87.87779y^2 - 284.24264y^3 \\
& + 463.83801y^4 - 369.81230y^5 + 115.08588y^6)x^5 \\
& + (-0.13189 + 14.60642y - 144.69672y^2 + 529.23363y^3 \\
& - 899.73602y^4 + 725.67077y^5 - 225.66361y^6)x^6 \\
& + (-0.30734 - 11.10747y + 144.89421y^2 - 565.76399y^3 \\
& + 982.58529y^4 - 797.70747y^5 + 248.00979y^6)x^7 \\
& + (0.29947 + 5.31976y - 82.06726y^2 + 330.24011y^3 \\
& - 579.34304y^4 + 472.44205y^5 - 147.08568y^6)x^8 \\
& + (-0.08325 - 1.22603y + 20.06377y^2 - 81.40275y^3 \\
& + 143.32172y^4 - 117.33319y^5 + 36.68467y^6)x^9. \tag{A.4}
\end{aligned}$$

Note that after plugging the 6th order polynomials into Eq. (2.5), the polynomials  $A$ ,  $B$ ,  $C$ , and  $D$  end up having slightly higher order and 249 coefficients, with 39 of them not independent.

## Acknowledgments

We have benefited from conversations with Pau Figueras, James Lucietti, and Toby Wiseman and greatly appreciate their sharing their detailed numerical data with us for comparison. CC acknowledges an Avadh Bhatia Postdoctoral Fellowship at the University of Alberta. This research was also supported in part by the Natural Sciences and Engineering Research Council of Canada.

## References

- [1] L. Randall and R. Sundrum, *An alternative to compactification*, 1999 Phys. Rev. Lett. **83**, 4690 [hep-th/9906064].
- [2] G. Nordström, 1912 Phys. Zeit. **13**, 1126.
- [3] T. Kaluza, *On the problem of unity in physics* (in German and English), 1921 Sitzungsber Preuss. Akad. Wiss. (Berlin) **966**.
- [4] O. Klein, *Quantum theory and five-dimensional theory of relativity*, 1926 Zeit. f. Phys. **37**, 895.
- [5] V. A. Rubakov and M. E. Shaposhnikov, *Do we live inside a domain wall?*, 1983 Phys. Lett. B. **125**, 136.
- [6] J. Polchinski, *Dirichlet-Branes and Ramond-Ramond charges*, 1995 Phys. Rev. Lett. **75**, 4724 [hep-th/9510017].
- [7] L. Randall and R. Sundrum, *A large mass hierarchy from a small extra dimension*, 1999 Phys. Rev. Lett. **83**, 3370 [hep-ph/9905221].
- [8] R. Emparan, G. T. Horowitz, and R. C. Myers, *Exact description of black holes on branes*, 2000 J. High Energy Phys. **01**, 007 [hep-th/9911043].
- [9] J. F. Plebanski and M. Demianski, *Rotating, charged, and uniformly accelerating mass in general relativity*, 1976 Ann. Phys. (N.Y.) **98**, 98.
- [10] R. Emparan, A. Fabbri, and N. Kaloper, *Quantum black holes as holograms in AdS braneworlds*, 2002 JHEP **8**, 43 [hep-th/0206155].
- [11] T. Tanaka, *Classical black hole evaporation in Randall-Sundrum infinite braneworld*, 2002 Prog. Theor. Phys. Suppl. **148**, 307 [gr-qc/0203082].
- [12] A. L. Fitzpatrick, L. Randall, and T. Wiseman, *On the existence and dynamics of braneworld black holes*, 2006 JHEP **11**, 033 [hep-th/0608208].
- [13] H. Kudoh, T. Tanaka, and T. Nakamura, *Small localized black holes in a braneworld: Formulation and numerical method*, 2003 Phys. Rev. D **68**, 024035 [gr-qc/0301089].
- [14] H. Kudoh, *Thermodynamic properties of small localized black holes*, 2003 Prog. Theor. Phys. **110**, 1059 [hep-th/0306067].
- [15] H. Yoshino, *On the existence of a static black hole on a brane*, 2009, JHEP **01**, 068 [gr-qc/0812.0465].
- [16] B. Kleihaus, J. Kunz, E. Radu, and D. Senkbeil, *Electric charge on the brane?*, 2011 Phys. Rev. D **83**, 104050 [gr-qc/1103.4758].
- [17] N. Dadhich, R. Maartens, P. Papadopoulos, and V. Rezanian, *Black holes on the brane*, 2000 Phys. Lett. B **487**, 1 [hep-th/0003061].
- [18] P. R. Anderson, R. Balbinot, and A. Fabbri, *Cutoff Anti-de Sitter space/conformal-field-theory duality and the quest for braneworld black holes*, 2005 Phys. Rev. Lett. **94**, 061301 [hep-th/0410034].

- [19] A. Fabbri, S. Farese, J. Navarro-Salas, G. J. Olmo, and H. Sanchis-Alepuz, *Semiclassical zero-temperature corrections to Schwarzschild spacetime and holography*, 2006 Phys. Rev. D **73**, 104023 [hep-th/0512167].
- [20] D. C. Dai and D. Stojkovic, *Analytic solution for a static black hole in RSII model*, 2011 Phys. Lett. B **704**, 354-359 [gr-qc/1004.3291].
- [21] P. Kanti, I. Olasagasti, and K. Tamvakis, *Quest for localized 4-D black holes in brane worlds. II. Removing the bulk singularities*, 2003 Phys. Rev. D **68**, 124001 [hep-th/0307201].
- [22] R. Gregory, *Braneworld black holes*, 2009 Lect. Notes Phys., **769**, 259-298 [hep-th/0804.2595].
- [23] P. Figuras and T. Wiseman, *Gravity and large black holes in Randall-Sundrum II braneworlds*, 2011 Phys. Rev. Lett. **107**, 081101 [hep-th/1105.2558].
- [24] P. Figuras, J. Lucietti, and T. Wiseman, *Ricci solitons, Ricci flow, and strongly coupled CFT in the Schwarzschild Unruh or Boulware vacua*, 2011 Class. Quantum Grav. **28**, 215018 [hep-th/1104.4489].
- [25] S. Abdolrahimi, C. Céline Cattoën, D. N. Page, and S. Yaghoobpour-Tari, *Large Randall-Sundrum II black holes*, 2012 arXiv:1206.0708 [hep-th].
- [26] A. Chamblin, S.W. Hawking and H.S. Reall, *Brane-world black holes*, 2000 Phys. Rev. **D61**, 065007.
- [27] S. Abdolrahimi and A. A. Shoom, *Geometric properties of static EMdL horizons*, 2011 Phys. Rev. D **83**, 104023 [hep-th/1103.1171].
- [28] C. Fefferman, C. R. Graham, *Conformal invariants*, Élie Cartan et les Mathématiques d'aujourd'hui, Astérisque, hors série, Soc. Math. France, Paris, pp. 95-116 (1985).
- [29] C.R. Graham, *Volume and area renormalizations for conformally compact Einstein metrics*, 19th Winter School on Geometry and Physics, Srni, Czech Republic, 1999 [math-dg/9909042].
- [30] S. de Haro, K. Skenderis, and S. N. Solodukhin, *Holographic reconstruction of spacetime and renormalization in the AdS/CFT correspondence*, 2001 Commun. Math. Phys. **217**, 595 [hep-th/0002230].